Journal of Materials Chemistry C

# Electronic Shell Structure, Self-Trapped Exciton, and Defect-Bound Exciton in Li2B12H12

| | |
|---|---|
| Journal: | *Journal of Materials Chemistry C* |
| Manuscript ID | TC-ART-07-2019-004150.R2 |
| Article Type: | Paper |
| Date Submitted by the Author: | 10-Oct-2019 |
| Complete List of Authors: | Du, Mao Hua ; Oak Ridge National Laboratory<br>Shi, Hongliang; Beihang University, Department of Physics<br>Zhang, Shengbai; Rensselaer Polytechnic Institute, |
| | |

# Electronic Shell Structure, Self-Trapped Exciton, and Defect-Bound Exciton in $Li_2B_{12}H_{12}$

Mao-Hua Du[1*], Hongliang Shi[2], S. B. Zhang[3]

[1]Materials Science and Technology Division, Oak Ridge National Laboratory, Oak Ridge, TN 37831, USA

[2]Key Laboratory of Micro-Nano Measurement-Manipulation and Physics (Ministry of Education), Department of Physics, Beihang University, Beijing 100191, China

[3]Department of Physics, Applied Physics, and Astronomy, Rensselaer Polytechnic Institute, Troy, NY, 12180

Keywords: $Li_2B_{12}H_{12}$; Luminescence; Exciton; Defect; Neutron scintillator; DFT calculation

*Corresponding Author: Mao-Hua Du (mhdu@ornl.gov)

**Abstract**

First-principles study of electronic structure, excitons, and defects in $Li_2B_{12}H_{12}$ reveal unique photophysical properties of $Li_2B_{12}H_{12}$ and its potential as a neutron scintillator material. We identify the electronic shell structure in $(B_{12}H_{12})^{2-}$, which gives rise to strong chemical stability of $(B_{12}H_{12})^{2-}$ and a large band gap of $Li_2B_{12}H_{12}$. Based on hybrid functional calculations, we show that excitons in $Li_2B_{12}H_{12}$ are strongly self-trapped and predict that the exciton excitation and emission are both in the UV range and are not related to the bright blue emission observed in experiment. The experimentally observed blue emission in $Li_2B_{12}H_{12}$ is likely due to the emission of excitons bound to hydrogen vacancies. The calculated strong localization and large exciton trapping energy at hydrogen vacancies indicate enhanced radiative recombination, while the calculated large Stokes shift suggests that the self-absorption and the resonance transfer of the excitation energy may be suppressed. These properties should promote efficient defect emission at room temperature. The efficient defect emission, combined with the large thermal neutron capture cross-section by Li and B and the efficient energy transfer between fast neutrons and H, suggest potential applications of $Li_2B_{12}H_{12}$ as a thermal or fast neutron scintillator. Optical characterization of $V_H$ may also be used to monitor H and Li concentrations in $Li_2B_{12}H_{12}$-based hydrogen storage material and solid-state electrolyte in Li batteries.

## I. Introduction

Metal boranes are a large family of compounds with unique chemical bonding[1] and diverse functionalities.[2, 3] $Li_2B_{12}H_{12}$ and related metal boranes and carboranes have received intensive interests for their wide range of applications, including inorganic solid-state electrolyte for battery technologies,[2, 3, 4-7] hydrogen storage,[2, 3,8, 9] and neutron capture therapy of cancer.[10, 11] Recently, $Li_2B_{12}H_{12}$ has also been found to exhibit interesting photophysical properties, which suggest potential applications as luminescent down-conversion dye.[12] However, different photoluminescence (PL) spectra have been reported and the origin of the luminescence (whether from excitons or defects/impurities) is still under debate. [12-14]

$Li_2B_{12}H_{12}$ contains anionic $(B_{12}H_{12})^{2-}$ clusters, which are separated from each other by $Li^+$ countercations. The resulting localized electronic states at $(B_{12}H_{12})^{2-}$ clusters and/or defects may trap excitons, leading to efficient self-activated luminescence.[15-18] Recent studies on low-dimensional materials, which are self-activated luminescent materials, have demonstrated high photoluminescence quantum efficiencies (PLQEs) (near unity in some cases) for self-trapped exciton (STE) emission.[16, 17, 19-28] Both STE and defect-related emissions have been reported in low-dimensional compounds.[17, 24] In this work, we studied the electronic structure as well as the excitation and emission of self-trapped and defect/impurity-bound excitons in $Li_2B_{12}H_{12}$. The highly symmetric icosahedral structure of $(B_{12}H_{12})^{2-}$ leads to an electronic shell structure with a large band gap. Our calculations of exciton and defect emissions suggest that the experimentally observed bright blue emission is not due to excitons but likely the result of the defect emission. On the other hand, the observed weak UV emission may result from the parity-forbidden exciton emission. We further propose that the combination of the strong neutron capture capability of Li and B and the efficient luminescence renders $Li_2B_{12}H_{12}$ a potential neutron scintillator material,

which may be used for thermal or fast neutron detection. High-efficiency neutron detection is an important technology that finds applications in areas such as high energy physics, non-proliferation of special nuclear materials, nuclear energy, oil-well logging, etc.[29]

$^{6}_{3}Li$ and $^{10}_{5}B$ have significant thermal neutron capture cross sections of 940 barn and 3835 barn, respectively.[30] Thus, Li and B compounds have been extensively studied as thermal neutron scintillators.[29] $Li_2B_{12}H_{12}$ has high concentrations of both Li and B ($9.11 \times 10^{21}$ $cm^{-3}$ and $5.46 \times 10^{22}$ $cm^{-3}$, respectively). In comparison, LiI and $Cs_2LiYCl_6$, the two Li-containing solid-state neutron detector materials, have Li concentrations of $1.84 \times 10^{22}$ $cm^{-3}$ and $3.47 \times 10^{21}$ $cm^{-3}$, respectively. The Li concentration in $Li_2B_{12}H_{12}$ is comparable to those in LiI and $Cs_2LiYCl_6$, while the concentration of B, which has a higher thermal neutron capture cross section than Li, is significantly higher. As a result, $Li_2B_{12}H_{12}$ should be more efficient in capturing thermal neutrons than LiI and $Cs_2LiYCl_6$. $Li_2B_{12}H_{12}$ has a low density of 1.23 $g/cm^3$, much lower than those of LiI and $Cs_2LiYCl_6$, which are 4.13 $g/cm^3$ and 3.33 $g/cm^3$, respectively. The low density of $Li_2B_{12}H_{12}$ is highly desirable for reducing sensitivity to background gamma rays. Furthermore, hydrogen in $Li_2B_{12}H_{12}$ can absorb the energy of fast neutrons efficiently; thus, the hydrogen-rich $Li_2B_{12}H_{12}$ may be interesting as a fast neutron scintillator as well.

The fast neutrons transfer their kinetic energy to protons through elastic scattering. For the slower thermal neutrons, the absorption by $^{6}_{3}Li$ and $^{10}_{5}B$ leads to prompt nuclear reactions [$^{6}_{3}Li + {}^{1}_{0}n \rightarrow {}^{4}_{2}He$ (2.05 MeV) + $^{3}_{1}H$ (2.73 MeV); $^{10}_{5}B + {}^{1}_{0}n \rightarrow {}^{4}_{2}He$ (1.013 MeV) + $^{7}_{3}Li$ (1.776 MeV)],[29] which produce secondary charged particles with significant energy. In either case, if the energy deposited into $Li_2B_{12}H_{12}$ leads to efficient light emission, $Li_2B_{12}H_{12}$ would be interesting as a neutron scintillator.

## II. Computational Methods

All calculations on $Li_2B_{12}H_{12}$ were based on density functional theory (DFT) implemented in the VASP code.[31] The interaction between ions and electrons was described by projector augmented wave method.[32] The kinetic energy cutoff of 499 eV for the plane-wave basis was used for all calculations except the dielectric constant calculation, in which a higher energy cutoff of 624 eV was used. The reciprocal-space integrations were performed on a 2 × 2 × 2 k-point mesh. Experimental lattice parameters of $Li_2B_{12}H_{12}$ (space group *Pa* -3; a = 9.57713 Å) [33] were used while the atomic positions were fully relaxed until the residual forces were less than 0.02 eV/ Å.

Electronic band structure and density of states (DOS) of $Li_2B_{12}H_{12}$ were calculated using Perdew−Burke−Ernzerhof (PBE) exchange-correlation functional[34] while the exciton and defect properties were treated by using more advanced hybrid PBE0 functional,[35] which has 25% non-local Fock exchange. The inclusion of a fraction of Fock exchange significantly improves the band gap energy[35-37] and the description of charge localization in insulators.[38-42]

The electronic shell structure of the $(B_{12}H_{12})^{2-}$ cluster was analyzed by calculating the auxiliary radial functions[43]

$$F_l(r) = \sum_m \left| \int_\Omega Y_{lm}^*(\theta,\phi)\,\Psi(\mathbf{r})\,d\Omega \right|^2 , \quad (1)$$

where $\Psi(\mathbf{r})$ is the wavefunction and $Y_{lm}(\theta, \phi)$ is the spherical harmonic function. The integration in Eq. (1) was carried out over the surface of a sphere of radius $r$ centered at the middle of the cluster. The above wavefunction analysis of the charged $(B_{12}H_{12})^{2-}$ cluster was performed using the BOMD code[44] with Troullier-Martin pseudopotential.[45]

The total energy of an exciton was calculated by fixing the occupation numbers of the electron and hole-occupied eigenlevels [Δ self-consistent field (ΔSCF) method[46-48]]. The ΔSCF method has formally been justified for general excited states by extending the Kohn-Sham formalism to include excited states.[47] The ΔSCF method can be easily used in $Li_2B_{12}H_{12}$ because the electron and hole are both localized on a single $(B_{12}H_{12})^{2-}$ cluster and each occupies one single eigenlevel deep inside the band gap.[16] The ΔSCF method combined with the hybrid PBE0 functional allows excited-state structural relaxation and has shown accurate results in exciton excitation and emission energies in many compounds.[16-18, 20, 21, 24, 27, 49] Between the two popular hybrid functionals (PBE0 and HSE functionals), the PBE0 band gap error is usually smaller in large-gap insulators but larger in semiconductors with medium to small band gaps.[37, 42, 50] We used PBE0 functional in this study because $Li_2B_{12}H_{12}$ is an insulator with a large band gap (see Sec. III-A).

Following the Franck-Condon principle, the exciton excitation and emission energies were obtained by calculating the total energy differences between the excited and the ground states using PBE0-optimized ground-state and excited-state structures, respectively. Although the spin-triplet exciton is slightly more stable, the spin-singlet exciton was considered in the excited-state calculation because the spin-orbit coupling, which can enable intersystem crossing between singlet and triplet excitons, is weak in $Li_2B_{12}H_{12}$, which consist of only light elements. The exciton binding energy relative to a free electron and a free hole was calculated by

$$\Delta E_b = E(\mathrm{GS}) + E_g - E(\mathrm{exciton}), \quad (2)$$

where $E$(GS) and $E$(exciton) are the total energies of the ground state and the exciton, respectively, and $E_g$ is the band gap.

The charge transition level $\varepsilon(\mathrm{q}/\mathrm{q}')$ of a defect was determined by the Fermi level at which the formation energy of the defect with the charge state *q* is equal to that with the charge state *q*'[51]:

$$\varepsilon(\mathrm{q}/\mathrm{q}') = \frac{E_{D,q'} - E_{D,q}}{q - q'}, \quad (3)$$

where $E_{D,q}$ ($E_{D,q'}$) is the total energy of the supercell that contains the relaxed structure of a defect at charge state *q* (*q'*). The binding energies of hole and electron polarons (or the energies of hole and electron polarons relative to those of free hole and free electron) are $\varepsilon_{hole-pol}(+/0) - \varepsilon_V$ and $\varepsilon_c - \varepsilon_{electron-pol}(0/-)$, respectively.[42] Here, $\varepsilon_V$ and $\varepsilon_c$ are the energies of the valence band maximum (VBM) and the conduction band minimum (CBM), respectively. $\varepsilon_{hole-pol}(+/0)$ and $\varepsilon_{electron-pol}(0/-)$ are the transition levels for the hole and the electron polarons, respectively. When calculating the transition levels for polarons using Eq. 3, the structure for the neutral charge state is simply the structure of the defect-free material. Therefore, the binding energies of hole and electron polarons are $E_0 - E_{hole-pol} - \varepsilon_v$ and $\varepsilon_c - E_{electron-pol} + E_0$, where $E_0$ is the energy of the neutral defect-free supercell and $E_{hole-pol}$ and $E_{electron-pol}$ are the energies of the supercells that contain relaxed structures of hole and electron polarons, respectively. The image-charge and potential alignment corrections were applied to the total energies of the charged defects and polarons.[52] The dielectric constant was calculated for the purpose of estimating the image charge correction.[56] The calculated static dielectric constant in $Li_2B_{12}H_{12}$ is 7.06. The electronic and ionic contributions to the static dielectric constant are 3.12 and 3.94, respectively.

## III. Results and Discussion

### A. Electronic structure

Figure 1 shows the electronic band structure and DOS of $Li_2B_{12}H_{12}$ calculated using the PBE exchange-correlation functional. The band gap is direct at the Γ point. The calculated PBE band gap is 5.74 eV, which is expected to be underestimated due to the well-known band gap error of the PBE calculation. The hybrid PBE0 calculation increases the band gap to 7.63 eV. The projected DOS shown in Figure 1(b) shows that both valence and conduction bands are made up of the molecular orbitals (MOs) of $(B_{12}H_{12})^{2-}$. The large band gap indicates the exceptional stability of the $(B_{12}H_{12})^{2-}$ molecule, which exhibits electronic shell structure as shown below.

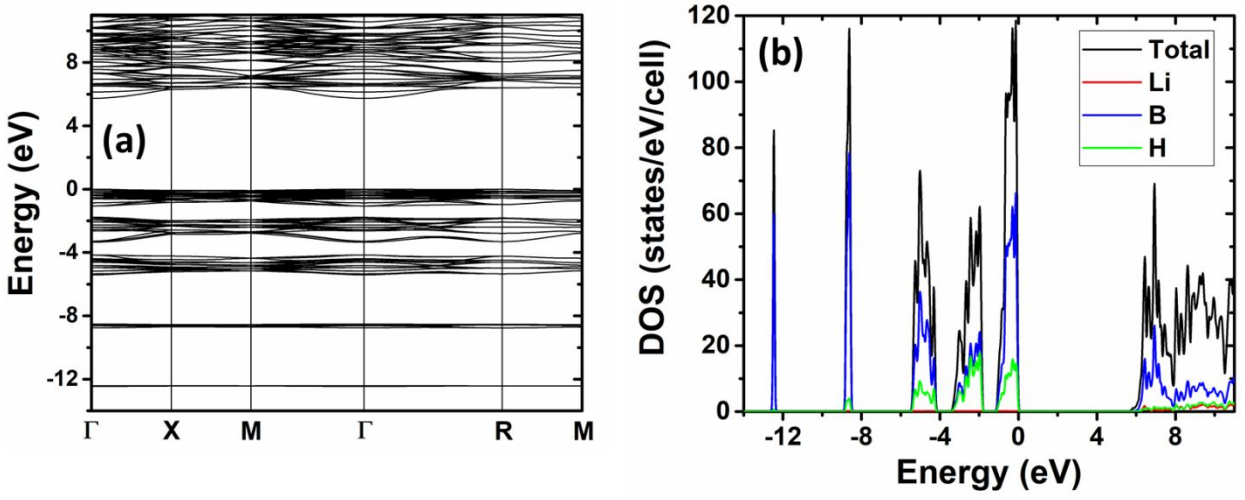


Figure 1. Electronic band structure (a) and density of states (DOS) (b) of $Li_2B_{12}H_{12}$ obtained by the PBE calculation. Note that the band gap is underestimated. The hybrid PBE0 calculation increases the band gap to 7.63 eV. The energy of the valence band maximum is set to zero.

Figure 2(a) shows the energy levels of the occupied MOs of the $(B_{12}H_{12})^{2-}$ molecule. The comparison between Figure 1 and Figure 2(a) shows that the five occupied narrow bands in Figure 1 largely retain the molecular character of $(B_{12}H_{12})^{2-}$. The $(B_{12}H_{12})^{2-}$ molecule has the highly symmetric icosahedral structure; its 50 valence electrons (consisting of B 2s and 2p and H 1s electrons) occupy the $A_g$, $T_{1u}$, $H_g$, $A_g$, $T_{1u}$, $T_{2u}$, $H_g$, $G_u$ levels as shown in Figure 2(a). The

$(B_{12}H_{12})^{2-}$ molecule behaves somewhat like a superatom,[53, 54] exhibiting the electronic shell structure.[55] The occupied MOs in $(B_{12}H_{12})^{2-}$ in Figure 2(a) are labeled by $n$, $l$, and the symmetry, where $n$ is the number of radial nodes plus one, and $l$ is the angular momentum of the wave function. The $n$ and $l$ are determined by the auxiliary radial function $F_l(r)$ as calculated by Eq. 1. Figures 2(b)-(i) show $F_l(r)r^2$, as a function of $r$ for the occupied states shown in Fig. 2(a). We found, with only two exceptions [Fig. 2 (f) and (h)] (to be explained later), that each state here has a dominant angular momentum and is therefore labeled by only one set of $n$ and $l$. The icosahedral point group ($I_h$) splits the spherical harmonic $f$ state into $G_u$ and $T_{2u}$ states, and also split the $g$ state into $H_g$ and $G_g$ states. The $I_h$ point group, however, does not split the $p$ and $d$ states.

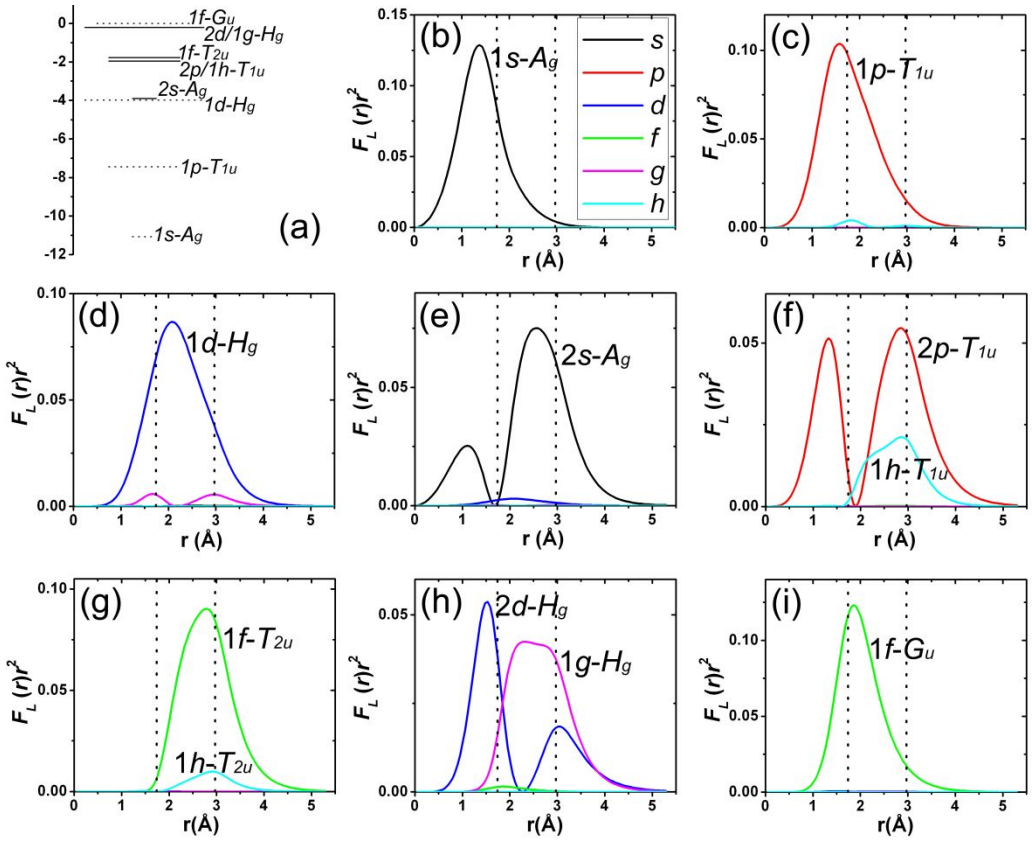


Figure 2. (a) Occupied energy levels of icosahedral $(B_{12}H_{12})^{2-}$ with the energy of the HOMO is set to zero. The energy levels in dotted line indicate the skeletal $B_{12}$ MOs while those in solid line

indicate the B-H MOs. (b)-(i) $F_l(r)r^2$, where $F_l(r)$ is the auxiliary radial function defined by Eq. 1, are shown for each occupied MO. The two dotted lines in (b)-(i) indicate the position of the B and H atoms, respectively.

From the wavefunction analysis, one can identify that (i) the 1*s*, 1*p*, 1*d*, and 1*f*-$G_u$ orbitals [shown by dotted lines in Fig. 2(a)] are the 13 MOs of $B_{12}$ (skeletal bonds of the $B_{12}$ cage), and (ii) the 2*s*, 2*p*/1*h*-$T_{1u}$, 1*f*- $T_{2u}$, and 2*d*/1*g*- $H_g$ orbitals are 12 B-H MOs that host 24 electrons.[56] Among the skeletal orbitals, the 1*d* and 1*f*-$G_u$ orbitals exhibit the characteristic three-center-two-electron (3c2e) bond[1] with triangular-shaped wavefuctions on the surface of the cage.[57]

Although the bonding in $(B_{12}H_{12})^{2-}$ molecule is not purely metallic (due to the covalent B-H bonds), the shell model[55] commonly used for metal clusters could still be a good starting point to analyzing the molecular stability, because the MOs for the skeletal bonds are all delocalized. We note that the total number of electrons for $(B_{12}H_{12})^{2-}$ is 50, which, within the square-well potential approximation,[55] is not a magic number for a stable metal cluster, because 50 electrons fill 1*s*, 1*p*, 1*d*, 2*s*, 2*p*, 1*f* states and five of the 1*g* states, leaving no energy gap. However, under the icosahedral potential of $(B_{12}H_{12})^{2-}$, the partially occupied 1*g* state splits into 1*g*-$H_g$ (occupied) and 1g-$G_g$ (empty), creating an energy gap. The gap is further widened significantly by the hybridization between the occupied 1*g*-$H_g$ states and the empty 2*d* states [see Fig. 2(h)]. Such hybridization lowers the occupied 2*d*/1*g*-$H_g$ bonding state below the 1*f*-$G_u$ state, which becomes the highest occupied molecular orbital (HOMO) for $(B_{12}H_{12})^{2-}$, and meanwhile raises the empty 2*d*/1*g*-$H_g$ anti-bonding state above the 3*s* state, which becomes the lowest unoccupied molecular orbitals (LUMO). Note that the strong hybridization of 2*d* and 1*g*-$H_g$ states of different angular momenta is allowed because they are B-H states under less spherical potential. Similarly, the

occupied 2*p* and the empty 1*h*-$T_{1u}$ states also hybridize strongly [see Fig. 2(f)] to further lower the energy and stabilize the $(B_{12}H_{12})^{2-}$ molecule.

The high symmetry of $(B_{12}H_{12})^{2-}$ leads to electronic shell structure as shown above and is also responsible for the enhanced stability of $(B_{12}H_{12})^{2-}$ relative to other experimentally observed *closo* boranes [$B_nH_n^{2-}$ $(6 \leq n \leq 11)$].[1] The hybridization of the B-H orbitals lowers the total energy and widens the HOMO-LUMO gap most effectively in $B_{12}H_{12}^{2-}$ due to its high-level orbital degeneracy, but less so in all other *closo* boranes (of lower symmetry). Also, the quasi-sphericality of $B_{12}H_{12}^{2-}$ allows for better itinerancy of the electrons on the boron cage surface, which is desirable for the resonant 3c2e skeletal bonding.[56]

**B. Exciton excitation, relaxation, and emission**

The small dispersion of both the valence and conduction bands in $Li_2B_{12}H_{12}$ as shown in Figure 1(a) indicates that the electronic coupling between the adjacent $(B_{12}H_{12})^{2-}$ molecules is weak. As a molecular crystal, the bond distortion in one $(B_{12}H_{12})^{2-}$ molecule does not affect bonding in adjacent $(B_{12}H_{12})^{2-}$ molecules significantly. The narrow bands and the weak inter-cluster coupling promote the formation of the STE, which is localized on one $(B_{12}H_{12})^{2-}$ cluster rather than delocalized. Figure 3 shows the partial charge density contours for the hole and the electron wavefunctions in a STE. As can be seen, the exciton is localized on the $B_{12}$ cage not on the B-H bonds. The hole is distributed on eight B-B-B triangles while the electron is mostly localized on six B-B bonds. The length of these six B-B bonds is decreased from 1.77Å in the ground state to 1.66 Å, whereas the side lengths of the eight hole-occupied B-B-B triangles are increased from 1.77 Ă to 1.85 Ă in average. The electron wavefunction distributed on the six B-

B bonds is polarized towards to the adjacent six Li cations, which are the vertices of a $Li_6$ octahedron.

The spin-allowed excitation creates spin-singlet excitons. The triplet exciton is calculated to be more stable than the singlet exciton by 0.08 eV. However, due to the weak spin-orbit coupling in $Li_2B_{12}H_{12}$, which consists of only light elements, the intersystem crossing is inefficient. Thus, we calculated the exciton emission energy based on the singlet exciton. The calculated exciton excitation and emission energies are 7.06 eV and 4.60 eV (based on the hybrid PBE0 calculation). The large Stokes shift of 2.46 eV is due to the strong excited-state relaxation as shown above, which lowers the exciton energy by 1.23 eV, indicating strong exciton self-trapping. The exciton binding energy relative to the free electron and hole for the unrelaxed and relaxed singlet exciton is calculated to be 0.57 eV and 1.79 eV, respectively, by using Eq. 2. Thus, free electrons and holes should not exist at room temperature due to the large exciton binding energy.

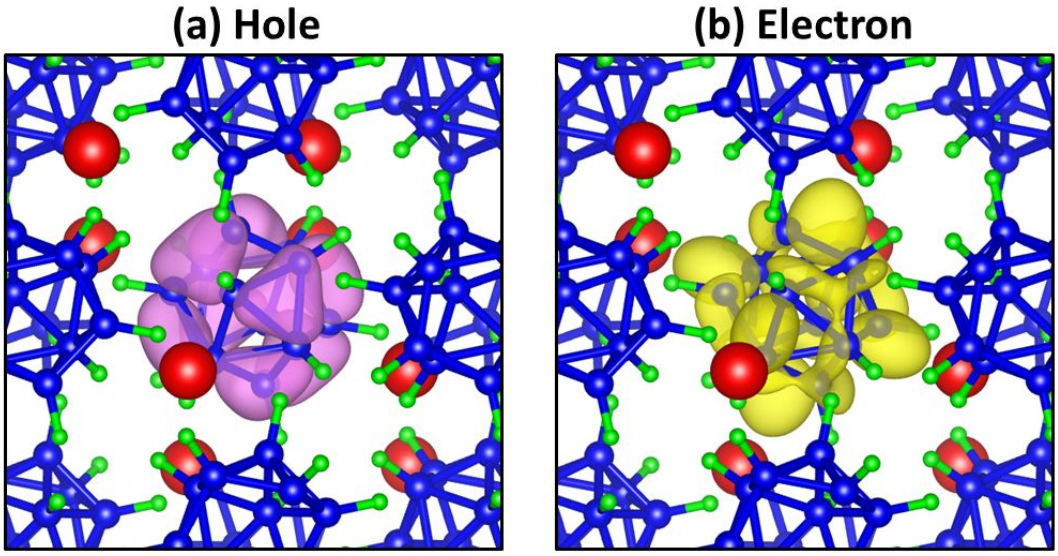


Figure 3. Partial charge density contours of the hole (a) and the electron (b) in a relaxed exciton in $Li_2B_{12}H_{12}$.

We have also calculated the binding energies of electron and hole polarons in $Li_2B_{12}H_{12}$ and studied exciton stability against dissociation to polarons. Our calculation shows a binding energy of 0.72 eV for a hole polaron, which is localized on one $(B_{12}H_{12})^{2-}$ cluster causing the expansion of the areas of the eight B-B-B triangles. However, the electron polaron is found to be less stable than a delocalized free electron by 0.12 eV. Thus, we calculated the exciton binding energy relative to a hole polaron and a free electron; the calculated binding energy is 1.07 eV, which is significant. These calculations show that the exciton in $Li_2B_{12}H_{12}$ should be stable against dissociation to polarons or free carriers at room temperature.

Table 1. The calculated excitation and emission energies for the self-trapped exciton and the excitons bound to hydrogen vacancies [at +1, 0, and -1 charge states ($V_H^+$, $V_H^0$, $V_H^-$)] and the $(B_{11}H_{14})^-$ impurity. The experimentally measured peak energies in excitation and emission spectra are also shown for both the blue[12] and UV[13] emissions in $Li_2B_{12}H_{12}$.

| | Excitation Energy (eV) | Emission Energy (eV) |
|---|---|---|
| Exciton | 7.06 | 4.60 |
| $V_H^+$ | 3.63 | 1.30 |
| $V_H^0$ | 4.54 | 1.92 |
| $V_H^-$ | 3.90 | 1.95 |
| $(B_{11}H_{14})^-$ | 5.82 | 1.89 |
| Exp. (blue emission[12]) | 3.65 | 2.64 |
| Exp. (UV emission[13]) | N/A | 3.54 |

The experimentally observed blue emission in solid-state $Li_2B_{12}H_{12}$ is centered at 470 nm (2.64 eV),[12] which is much lower than the PBE0-calculated exciton emission energy of 4.60 eV. (We have also tested another hybrid functional, i.e., the HSE functional,[36, 58] which results in the exciton emission energy that differs from the PBE0 result by only 0.01 eV.) Such large discrepancy suggests that the experimentally observed blue emission at 470 nm is not due to the exciton emission. The calculated exciton excitation and emission energies for $Li_2B_{12}H_{12}$ are both very high in the UV range, which directly result from the exceptional stability and the large band gap as discussed in Sec. III-A. The observed blue emission was shown to be bright at room temperature. Our calculated squared transition dipole moment between the electron and the hole states of a STE is near zero, 0.04 Debye$^2$ (due to the parity-forbidden transition), indicating a slow emission and possibly a weak emission. (Note that an inefficient optical transition does not necessarily result in a weak optical emission,[59] because a slow emission can still be intense as long as the nonradiative recombination of the exciton is inefficient.) Measuring the decay time of the blue emission would be useful for the understanding of the emission mechanism.

Paskevicius et al. reported a weak UV emission around 3.54 eV (350 nm) with a low PLQE of only 0.0002 by $Li_2B_{12}H_{12}$ in aqueous solution.[13] The weak UV emission reported in Ref. 13 is not visible to human eyes in contrast to the bright blue emission reported in Ref. 12. The reported UV emission energy of 3.54 eV is closer to but still significantly lower than the calculated exciton emission energy of 4.60 eV. However, the optical measurements were performed on $Li_2B_{12}H_{12}$ in aqueous solution while our calculations were based on solid-state $Li_2B_{12}H_{12}$; this may cause some discrepancy between calculated and measured results. The weak UV emission could be due to the parity-forbidden STE emission. However, we cannot rule out the possibility of emission by an unknown defect or impurity.

### C. Exciton trapping and emission at hydrogen vacancy

The observed low emission energy in $Li_2B_{12}H_{12}$[12] relative to the calculated band gap and exciton emission energy suggests that the emission may be related to defect levels inside the band gap. The sub-band-gap excitation energy used in the experiment (3.65 eV) is substantially lower than the calculated exciton excitation energy of 7.06 eV and, thus, cannot generate excitons. However, such excitation may excite defects, leading to defect-related luminescence. It has been shown that increasing temperature to a moderate level of 355 °C leads to a phase transition followed by hydrogen release and decomposition.[60, 61] Thus, hydrogen vacancy ($V_H$) may exist in significant quantity in $Li_2B_{12}H_{12}$ at room temperature, acting as luminescent centers.

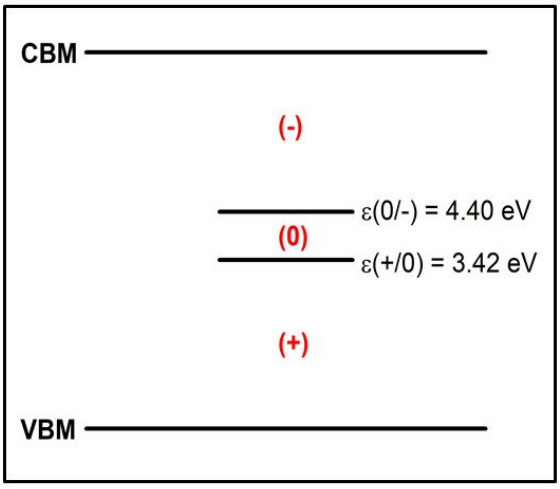


Figure 4. PBE0-calculated charge transition levels of $V_H$ in $Li_2B_{12}H_{12}$.

Removing a hydrogen atom from the $B_{12}H_{12}$ molecule results in a B dangling bond, which inserts a deep level inside the band gap. We find that $V_H$ is an amphoteric defect with its (+/0) and (0/-) charge transition levels located at $\varepsilon_{VBM}$ + 3.42 eV and $\varepsilon_{VBM}$ + 4.40 eV, respectively (Figure 4). The charge state of $V_H$ depends on the Fermi level of $Li_2B_{12}H_{12}$. A high

Fermi level favors $V_H^-$, whereas a low Fermi level favors $V_H^+$. In $Li_2B_{12}H_{12}$, the Fermi level is likely closer to the CBM rather than the VBM because the large electron affinity of $B_{12}H_{12}$[62] leads to a low VBM that makes hole generation energetically costly. The strong electronegativity of $B_{12}H_{12}$ favors the filling of the B dangling bond of the $V_H$ defect to form a lone pair, resulting in the negatively charged $V_H^-$. $(B_{12}H_{12})^{2-}$ is a large-sized anion carrying a small charge of -2, which is balanced by merely two small-sized $Li^+$ cations in $Li_2B_{12}H_{12}$. Therefore, there are plenty of interstitial spaces between $(B_{12}H_{12})^{2-}$ anions in $Li_2B_{12}H_{12}$, which can accommodate Li interstitials. These Li interstitials are electron donors that raise the Fermi level to favor the formation of $V_H^-$.

An exciton can be trapped by $V_H$, forming a $V_H$-bound exciton. Table 1 shows the PBE0-calculated excitation and emission energies for excitons bound to $V_H^+$, $V_H^0$, and $V_H^-$. The calculated excitation and emission energies of $V_H^-$-bound exciton agree reasonably well with the experimentally measured peak excitation and emission energies, suggesting that the blue emission observed in $Li_2B_{12}H_{12}$[12] is likely due to the $V_H^-$-bound exciton. The PBE0 calculation shows that the trapping of a STE by $V_H^-$ lowers the total energy by 2.80 eV; such large trapping energy indicates strong binding of the exciton to $V_H^-$. Figure 5 shows the partial charge density contours of the hole and electron wavefunctions in a $V_H^-$-bound exciton. The hole is trapped by the hydrogen vacancy defect on the B dangling bond, while the electron is distributed on the $B_{12}H_{12}$ surface, similar to the electron in a STE shown in Figure 3(b). The removal of a H from $B_{12}H_{12}$ breaks the inversion symmetry; therefore, the optical transition at $V_H^-$ is no longer parity forbidden; the calculated squared transition dipole moment is 78.9 Debye$^2$, compared to the near-

zero value (0.04 Debye[2]) for a STE. The large Stokes shift of $V_H$ emission as shown in Table 1 (the energy difference between the excitation and emission) suppresses self-absorption and excitation energy transport, potentially leading to efficient luminescence.[16]

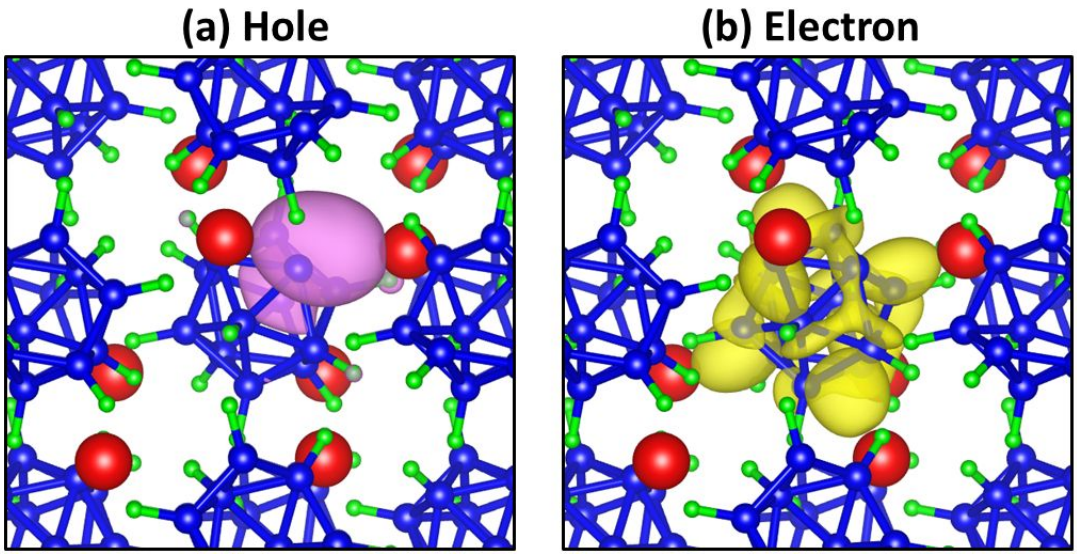


Figure 5. Partial density contours of the hole (a) and the electron (b) in a $V_H^-$-bound exciton in $Li_2B_{12}H_{12}$.

The excitation and emission spectra of $Li_2B_{12}H_{12}$ have been measured in solid-state $Li_2B_{12}H_{12}$ and $Li_2B_{12}H_{12}$ in water and various organic solvent (e.g., ethylene glycol).[12] It was found that the wavelength of the blue emission does not change significantly in the different forms of $Li_2B_{12}H_{12}$, whereas the excitation energy for dissolved $Li_2B_{12}H_{12}$ is significantly blue-shifted from that for solid-state $Li_2B_{12}H_{12}$. This may be caused by the change of the charge state of $V_H$ from -1 in solid-state $Li_2B_{12}H_{12}$ to neutral in dissolved $Li_2B_{12}H_{12}$ as suggested by the higher excitation energy of $V_H^0$ than that of $V_H^-$ in Table 1. The exciton trapping by $V_H^0$ can lead to two outcomes. One is that the hole is localized on the B dangling bond while the electron is localized on the $B_{12}$ cage, which is effectively a $V_H^+$ bound with an electron polaron. In the second

scenario, the electron is localized on the B dangling bond while the hole is localized on the $B_{12}$ cage, which is effectively a $V_H^-$ bound with a hole polaron. The calculated trapping energies of the above two $V_H^0$-bound excitons are 2.13 eV and 2.51 eV, respectively. Thus, the exciton trapping by $V_H^0$ should lead to the formation of a $V_H^-$ bound with a hole polaron. Our calculations show that the emission energy of the $V_H^0$-bound exciton is close to that of $V_H^-$ while the excitation energy of the $V_H^0$-bound exciton is significantly blue-shifted from that of $V_H^-$ (see Table 1). Therefore, the stable charge states of $V_H$ in solid state and dissolved $Li_2B_{12}H_{12}$ are likely to be -1 and neutral, respectively. The experiment showed that the emission energy is not sensitive to strong acid or strong basic conditions,[12] which also suggest that neutral $V_H^0$ is likely responsible for the blue emission in $Li_2B_{12}H_{12}$ in solution. The charged $V_H$ may easily be terminated by charged species in solution.

We have also studied the Li vacancy ($V_{Li}$) and found it is a shallow acceptor. The exciton bound to $V_{Li}$ is a weakly perturbed STE still localized at $(B_{12}H_{12})^{2-}$, whose excitation and emission energies are close to those for an isolated STE and, thus, should not account for the blue emission observed in experiment.

**D. $(B_{11}H_{14})^-$ and $(BH_4)^-$ impurities**

It was previously suggested that impurities, such as $(B_{11}H_{14})^-$ and $(BH_4)^-$, may be responsible for the visible light emission in $Li_2B_{12}H_{12}$.[13] We studied $(B_{11}H_{14})^-$ and $(BH_4)^-$ in $Li_2B_{12}H_{12}$ by replacing a $(B_{12}H_{12})^{2-}$ anion by $(B_{11}H_{14})^-$ and $(BH_4)^-$, respectively; therefore, these are +1 charged defects in $Li_2B_{12}H_{12}$. $(BH_4)^-$ is a very stable anion with four strong B-H covalent bonds and a large energy gap. As a result, $(BH_4)^-$ does not introduce impurity levels in the band

gap of $Li_2B_{12}H_{12}$ and cannot trap an exciton for luminescence. On the other hand, $(B_{11}H_{14})^-$ does insert deep levels within the band gap of $Li_2B_{12}H_{12}$. The calculated excitation and emission energies for $(B_{11}H_{14})^-$ in $Li_2B_{12}H_{12}$ are given in Table 1; the calculated excitation energy of 5.82 eV is too high compared to the experimentally measured excitation energy (3.65 eV) for the blue emission[12] while the calculated emission energy of 1.89 eV is too low compared to the observed UV emission (3.54 eV)[13]. Thus, $(B_{11}H_{14})^-$ is unlikely the origin of the observed blue[12] or UV[13] emission in $Li_2B_{12}H_{12}$, but could be related to the broad visible light emission observed in an impurity-rich sample of $Li_2B_{12}H_{12}$.[13]

### E. $Li_2B_{12}H_{12}$ as a neutron scintillator

As discussed above, $Li_2B_{12}H_{12}$ should be an efficient neutron absorber, which is a prerequisite for a neutron scintillator; another important prerequisite is the efficient light emission under ionizing radiation. Ionizing radiation generates excitons. The narrow conduction and valence bands in $Li_2B_{12}H_{12}$ lead to strong exciton self-trapping as shown in Sec. III-B, which should stabilize STEs at room temperature.[15] A STE can be further trapped by $V_H$ with a large trapping energy and the large Stokes shift of the $V_H$ emission is desirable for efficient light emission as discussed in Sec. III-C. A H-poor growth condition should help create $V_H$ and a Li-rich condition should promote the formation of $V_H^-$. The longer-wavelength emission of $V_H^+$ is less desirable because a photomultiplier tube has a lower quantum efficiency for the long wavelength red emission.

### F. Monitoring dynamic H and Li concentrations in $Li_2B_{12}H_{12}$

The emission intensity of the $V_H$-bound exciton is correlated to the density of $V_H$, [$V_H$]. Thus, the characteristic $V_H$ emission can be used to monitor the charging and discharging dynamics of $Li_2B_{12}H_{12}$ for hydrogen storage. Also, the densities of $V_H^-$ and $V_H^+$ are strongly affected by the Fermi level of $Li_2B_{12}H_{12}$, which in turn is affected by the density of the Li interstitial [$Li_i$]. As [$Li_i$] increases, the Fermi level should increase; consequently, [$V_H^-$] increases, [$V_H^+$] decreases, while [$V_H^0$] does not change. Since $V_H^+$, $V_H^0$, and $V_H^-$ have their characteristic optical excitation and emission energies (as shown in Table 1), by monitoring the relative intensities of their emission, one can monitor [$Li_i$] in $Li_2B_{12}H_{12}$ electrolyte during the charging and discharging processes in the Li battery. Thus, the characterization of the $V_H$ emission may be useful for the research and development of $Li_2B_{12}H_{12}$ as a hydrogen storage material or as a solid-state electrolyte material in Li batteries.

## IV. Conclusions

Hybrid DFT calculations are performed to gain fundamental understanding of the photophysical properties of $Li_2B_{12}H_{12}$. We found that $Li_2B_{12}H_{12}$ is a molecular crystal, in which the $(B_{12}H_{12})^{2-}$ molecule with the icosahedral symmetry exhibits an electronic shell structure. The weak inter-molecular electronic coupling leads to the small dispersion of both conduction and valence bands, promoting exciton self-trapping. The experimentally observed bright blue emission (excited by the sub-band-gap excitation) is assigned to the radiative recombination of the exciton bound to the hydrogen vacancy. The combination of the efficient luminescence and strong absorption of thermal neutrons by Li and B and fast neutrons by H indicate the potential application of $Li_2B_{12}H_{12}$ as a thermal or fast neutron scintillator. Optical characterization of $V_H$ may also provide a useful tool for monitoring H and Li concentrations in $Li_2B_{12}H_{12}$-based

hydrogen storage material and solid-state electrolyte in Li batteries. The insights gained in this study should be useful for the future design of new self-activated phosphors and scintillators.

## ACKNOWLEDGMENTS

We are grateful for the useful discussion with Zane W. Bell. The calculation of the electronic shell structure in $(B_{12}H_{12})^{2-}$ was supported by the U. S. Department of Energy, Office of Science, Basic Energy Sciences, Materials Sciences and Engineering Division. The calculation of the exciton and defect properties in $Li_2B_{12}H_{12}$ was supported by the ORNL Seed Money Fund. H. Shi was supported by the National Natural Science Foundation of China (NSFC) under Grants No.11604007 and the start-up funding at Beihang University. SBZ was supported by the US Department of Energy under Grant No. DE-SC0002623 for theoretical analysis.

## References:

1. R. B. King, *Chemical Reviews*, 2001, **101**, 1119-1152.
2. B. R. S. Hansen, M. Paskevicius, H.-W. Li, E. Akiba and T. R. Jensen, *Coordination Chemistry Reviews*, 2016, **323**, 60-70.
3. R. Mohtadi and S.-i. Orimo, *Nature Reviews Materials*, 2016, **2**, 16091.
4. S. Kim, N. Toyama, H. Oguchi, T. Sato, S. Takagi, T. Ikeshoji and S.-i. Orimo, *Chemistry of Materials*, 2018, **30**, 386-391.
5. M. Dimitrievska, P. Shea, K. E. Kweon, M. Bercx, J. B. Varley, W. S. Tang, A. V. Skripov, V. Stavila, T. J. Udovic and B. C. Wood, *Advanced Energy Materials*, 2018, **8**, 1703422.
6. K. E. Kweon, J. B. Varley, P. Shea, N. Adelstein, P. Mehta, T. W. Heo, T. J. Udovic, V. Stavila and B. C. Wood, *Chemistry of Materials*, 2017, **29**, 9142-9153.
7. Y. Yan, D. Rentsch, C. Battaglia and A. Remhof, *Dalton Transactions*, 2017, **46**, 12434-12437.
8. Q. Lai, T. Wang, Y. Sun and K.-F. Aguey-Zinsou, *Advanced Materials Technologies*, **0**, 1700298.
9. M. P. Pitt, M. Paskevicius, D. H. Brown, D. A. Sheppard and C. E. Buckley, *Journal of the American Chemical Society*, 2013, **135**, 6930-6941.
10. R. L. Moss, *Applied Radiation and Isotopes*, 2014, **88**, 2-11.
11. M. F. Hawthorne and A. Maderna, *Chemical Reviews*, 1999, **99**, 3421-3434.
12. J. A. Teprovich, H. Colón-Mercado, A. L. Washington Ii, P. A. Ward, S. Greenway, D. M. Missimer, H. Hartman, J. Velten, J. H. Christian and R. Zidan, *Journal of Materials Chemistry A*, 2015, **3**, 22853-22859.
13. M. Paskevicius, A. S. Jakobsen, M. Bregnhøj, B. R. S. Hansen, K. T. Møller, P. R. Ogilby and T. R. Jensen, *Journal of Materials Chemistry A*, 2019, **7**, 4185-4187.

14. J. A. Teprovich and R. Zidan, *Journal of Materials Chemistry A*, 2019, **7**, 4188-4189.
15. H. L. Shi and M. H. Du, *Phys. Rev. Appl.*, 2015, **3**, 054005.
16. D. Han, H. Shi, W. Ming, C. Zhou, B. Ma, B. Saparov, Y.-Z. Ma, S. Chen and M.-H. Du, *Journal of Materials Chemistry C*, 2018, **6**, 6398-6405.
17. G. Wu, C. Zhou, W. Ming, D. Han, S. Chen, D. Yang, T. Besara, J. Neu, T. Siegrist, M.-H. Du, B. Ma and A. Dong, *ACS Energy Letters*, 2018, **3**, 1443-1449.
18. H. Shi, D. Han, S. Chen and M.-H. Du, *Physical Review Materials*, 2019, **3**, 034604.
19. C. Zhou, H. Lin, Y. Tian, Z. Yuan, R. Clark, B. Chen, L. J. van de Burgt, J. C. Wang, Y. Zhou, K. Hanson, Q. J. Meisner, J. Neu, T. Besara, T. Siegrist, E. Lambers, P. Djurovich and B. Ma, *Chemical Science*, 2018, **9**, 586-593.
20. C. Zhou, M. Worku, J. Neu, H. Lin, Y. Tian, S. Lee, Y. Zhou, D. Han, S. Chen, A. Hao, P. I. Djurovich, T. Siegrist, M.-H. Du and B. Ma, *Chemistry of Materials*, 2018, **30**, 2374-2378.
21. R. Roccanova, A. Yangui, H. Nhalil, H. Shi, M.-H. Du and B. Saparov, *ACS Applied Electronic Materials*, 2019, **1**, 269-274.
22. C. Zhou, H. Lin, J. Neu, Y. Zhou, M. Chaaban, S. Lee, M. Worku, B. Chen, R. Clark, W. Cheng, J. Guan, P. Djurovich, D. Zhang, X. Lü, J. Bullock, C. Pak, M. Shatruk, M.-H. Du, T. Siegrist and B. Ma, *ACS Energy Letters*, 2019, **4**, 1579-1583.
23. T. Jun, K. Sim, S. Iimura, M. Sasase, H. Kamioka, J. Kim and H. Hosono, *Advanced Materials*, 2018, **30**, 1804547.
24. C. Zhou, H. Lin, Q. He, L. Xu, M. Worku, M. Chaaban, S. Lee, X. Shi, M.-H. Du and B. Ma, *Materials Science and Engineering: R: Reports*, 2019, **137**, 38-65.
25. B. M. Benin, D. N. Dirin, V. Morad, M. Wörle, S. Yakunin, G. Rainò, O. Nazarenko, M. Fischer, I. Infante and M. V. Kovalenko, *Angewandte Chemie International Edition*, 2018, **57**, 11329-11333.
26. R. Roccanova, M. Houck, A. Yangui, D. Han, H. Shi, Y. Wu, D. T. Glatzhofer, D. R. Powell, S. Chen, H. Fourati, A. Lusson, K. Boukheddaden, M.-H. Du and B. Saparov, *ACS Omega*, 2018, **3**, 18791-18802.
27. C. Zhou, H. Lin, H. Shi, Y. Tian, C. Pak, M. Shatruk, Y. Zhou, P. Djurovich, M.-H. Du and B. Ma, *Angewandte Chemie International Edition*, 2018, **57**, 1021.
28. M. D. Smith and H. I. Karunadasa, *Accounts of Chemical Research*, 2018, **51**, 619-627.
29. A. N. Caruso, *Journal of Physics: Condensed Matter*, 2010, **22**, 443201.
30. V. F. Sears, *Neutron News*, 1992, **3**, 26-37.
31. G. Kresse and J. Furthmüller, *Computational Materials Science*, 1996, **6**, 15-50.
32. G. Kresse and D. Joubert, *Physical Review B*, 1999, **59**, 1758.
33. C. Zhou, H. Lin, Y. Tian, Z. Yuan, R. J. Clark, B. Chen, B. van de Burgt, J. C. Wang, Y. Zhou, K. Hanson, Q. Meisner, J. Neu, T. Besara, T. Siegrist, E. Lambers, P. I. Djurovich and B. Ma, *Chemical Science*, 2018, **9**, 586-593
34. J. P. Perdew, K. Burke and M. Ernzerhof, *Physical review letters*, 1996, **77**, 3865.
35. J. P. Perdew, M. Emzerhof and K. Burke, *Journal of Chemical Physics*, 1996, **105**, 9982-9985.
36. J. Heyd, G. E. Scuseria and M. Ernzerhof, *Journal of Chemical Physics*, 2003, **118**, 8207-8215.
37. J. Paier, M. Marsman, K. Hummer, G. Kresse, I. C. Gerber and J. G. Angyan, *Journal of Chemical Physics*, 2006, **124**.
38. M.-H. Du and S. B. Zhang, *Physical Review B*, 2009, **80**, 115217.
39. A. Janotti, J. B. Varley, M. Choi and C. G. Van de Walle, *Physical Review B*, 2014, **90**, 085202.
40. A. Janotti, C. Franchini, J. B. Varley, G. Kresse and C. G. Van de Walle, *physica status solidi (RRL) – Rapid Research Letters*, 2013, **7**, 199-203.
41. L. Bjaalie, D. G. Ouellette, P. Moetakef, T. A. Cain, A. Janotti, B. Himmetoglu, S. J. Allen, S. Stemmer and C. G. V. d. Walle, *Applied Physics Letters*, 2015, **106**, 232103.
42. K. Biswas and M. H. Du, *Physical Review B*, 2012, **86**, 014102.

43. N. Troullier and J. L. Martins, *Physical Review B*, 1992, **46**, 1754-1765.
44. R. N. Barnett and U. Landman, *Physical Review B*, 1993, **48**, 2081-2097.
45. N. Troullier and J. L. Martins, *Physical Review B*, 1991, **43**, 1993-2006.
46. R. O. Jones and O. Gunnarsson, *Reviews of Modern Physics*, 1989, **61**, 689-746.
47. A. Görling, *Physical Review A*, 1999, **59**, 3359-3374.
48. A. Hellman, B. Razaznejad and B. I. Lundqvist, *The Journal of Chemical Physics*, 2004, **120**, 4593-4602.
49. M.-H. Du, *Journal of Materials Chemistry C*, 2019, **7**, 5710-5715.
50. A. J. Garza and G. E. Scuseria, *The Journal of Physical Chemistry Letters*, 2016, **7**, 4165-4170.
51. W. Ming, D. Yang, T. Li, L. Zhang and M.-H. Du, *Advanced Science*, 2018, **5**, 1700662.
52. S. Lany and A. Zunger, *Physical Review B*, 2008, **78**, 235104.
53. D. E. Bergeron, A. W. Castleman, T. Morisato and S. N. Khanna, *Science*, 2004, **304**, 84-87.
54. D. E. Bergeron, P. J. Roach, A. W. Castleman, N. O. Jones and S. N. Khanna, *Science*, 2005, **307**, 231-235.
55. W. A. de Heer, *Reviews of Modern Physics*, 1993, **65**, 611-676.
56. M.-H. Du, S. Saito and S. B. Zhang, *MRS Proceedings*, 2008, **1038**, 1038-O1005-1007.
57. R. B. King, T. Heine, C. Corminboeuf and P. v. R. Schleyer, *Journal of the American Chemical Society*, 2004, **126**, 430-431.
58. A. V. Krukau, O. A. Vydrov, A. F. Izmaylov and G. E. Scuseria, *Journal of Chemical Physics*, 2006, **125**, 224106.
59. M. H. Du, *Journal of Materials Chemistry C*, 2014, **2**, 2475-2481.
60. M. Paskevicius, M. P. Pitt, D. H. Brown, D. A. Sheppard, S. Chumphongphan and C. E. Buckley, *Physical Chemistry Chemical Physics*, 2013, **15**, 15825-15828.
61. N. Verdal, J.-H. Her, V. Stavila, A. V. Soloninin, O. A. Babanova, A. V. Skripov, T. J. Udovic and J. J. Rush, *Journal of Solid State Chemistry*, 2014, **212**, 81-91.
62. B. Pathak, D. Samanta , R. Ahuja and P. Jena, *ChemPhysChem*, 2011, **12**, 2423-2428.